

Beyond monoculture: polydisperse moment methods for sub-stellar atmosphere cloud microphysics

I. Examining properties of the exponential distribution

Elspeth K.H. Lee¹

¹Center for Space and Habitability, University of Bern, Gesellschaftsstrasse 6, CH-3012 Bern, Switzerland

Received 13 March 2025 / Accepted DD MM YYYY

ABSTRACT

Context. Observational data provided by JWST instruments continue to challenge theories and models of cloud formation in sub-stellar atmospheres, requiring more sophisticated approaches in an effort to understand their spatial complexity. However, to date, most cloud microphysical models using the moment method for sub-stellar atmospheres have assumed a monodisperse size distribution, neglecting polydisperse properties.

Aims. We aim to extend beyond the common assumption of a monodisperse size distribution and analyse cloud microphysical processes assuming an exponential distribution.

Methods. We derive expressions for the zeroth and first moments of condensation/evaporation and collisional growth processes under the assumption of an exponential size distribution. We then compare the differences between monodisperse and exponential distribution microphysics using a simple one-dimensional (1D) column model applied to a Y-dwarf KCl cloud scenario.

Results. We find that adopting an exponential distribution modifies condensation/evaporation rates by a factor of ≈ 0.9 and collisional growth rates by factors of ≈ 1.1 ($Kn \ll 1$) and ≈ 1.6 ($Kn \gg 1$) for Brownian coagulation and ≈ 0.85 for gravitational coalescence, compared to the monodisperse case. In our specific test cases, we find relative differences of a maximum 40% in total number density and 10% in mean radius of the cloud particles between the monodisperse and exponential distributions.

Conclusions. Our results offer a simple way to take into account an assumed exponential size distribution for sub-stellar atmospheric cloud microphysics using the two-moment method. In follow up studies, we will examine more complex distributions, such as the log-normal and gamma distributions, that require more than two moments to characterise self-consistently.

Key words. Planets and satellites: atmospheres – Methods: numerical

1. Introduction

The cloud particle size distribution plays a pivotal role in setting the observational properties of atmospheres that contain a cloud component, as the total opacity of the cloud is weighted by the individual contribution of each particle size to the size distribution. Further knock-on effects, affecting the thermal structure of the atmosphere through feedback with the radiative-transfer properties of the atmospheres, which, for example, in the case for brown dwarf atmospheres, can trigger local convection (e.g. [Tan & Showman 2019](#)) leading to changes in local chemical compositions (e.g. [Lee et al. 2024](#)). This makes the consideration and accurate modelling of cloud properties a key component of contemporary exoplanet and brown dwarf atmospheric modelling.

Exponential size distributions have been used for modelling Earth-based clouds, particularly raindrops, for decades since [Marshall & Palmer \(1948\)](#) proposed an exponential function as a best fit to observed raindrop data. Exponential distributions have consistently been applied to model raindrops and snow in the Earth atmosphere literature (e.g. [Pruppacher & Klett 1978](#); [Lin et al. 1983](#); [Hong & Lim 2006](#); [Seifert 2008](#); [Morrison et al. 2020](#)), with these schemes being used in general circulation models (GCMs) and other atmosphere simulation efforts such as mesoscale and large eddy simulations. However, for exoplanet and brown dwarf atmospheres the exact particle size distribution is unknown and is currently not directly measurable with suffi-

cient accuracy. Therefore, instead of parametrisation and fitting from in-situ data, as typically performed for Earth water clouds, it is advisable to develop theories and models in a generally applicable manner and self-consistent within their specific assumptions.

The moment (or bulk) method evolves integrated quantities of the particle size distribution over time, considering how cloud microphysical processes such as nucleation, condensation, evaporation, and collisions affect these quantities. The moment method is in contrast to the bin/spectral method which directly integrates a discretised grid of particle sizes or masses. A well used example of a bin model for sub-stellar objects is the 1D CARMA model (e.g. [Gao et al. 2018](#); [Powell et al. 2019](#)). However, the bin method is typically too computationally expensive to couple to large scale hydrodynamic models such as GCMs with contemporary resources, making development of moment schemes a useful middle-ground between computational efficiency and understanding the spacial time evolution of cloud microphysics.

Examples of moment methods used in sub-stellar atmosphere literature context ranges from 1D static approaches (e.g. [Woitke & Helling 2004](#); [Helling et al. 2008](#)), 1D time-dependent approaches (e.g. [Ohno & Okuzumi 2017](#); [Woitke et al. 2020](#)) to 3D time-dependent methods (e.g. [Lee et al. 2016](#); [Lines et al. 2018](#); [Lee 2023](#)). Several studies on sub-stellar atmospheres have employed multiple moment methods derived for monodis-

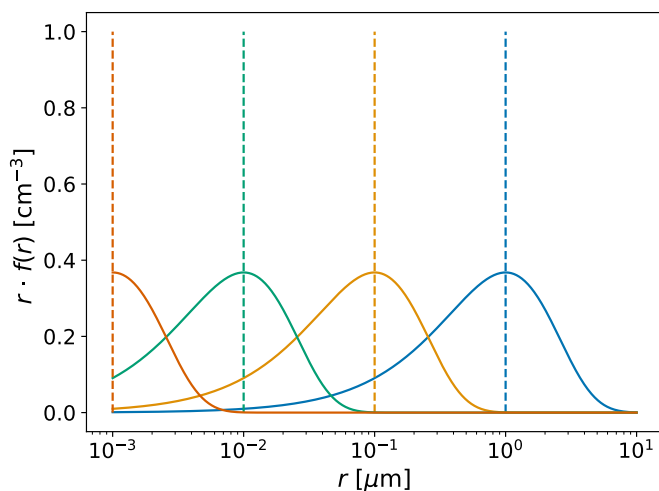


Fig. 1. Visualisation of the exponential size distribution compared against a monodisperse size distribution. This shows exponential distributions with (solid lines) $\lambda = 10^{-3}$ (red), 10^{-2} (green), 0.1 (orange) and 1 (blue) μm assuming $N_c = 1 \text{ cm}^{-3}$, with the equivalent monodisperse distribution (dashed lines). Overall, the exponential distribution enhances the representation of smaller particle sizes relative to the monodisperse distribution.

perse size distributions and subsequently reconstructed the particle size distribution using the moment solutions (e.g. Helling et al. 2008; Stark et al. 2015; Lee 2023).

Previous efforts typically assumed a delta function for a monodisperse size distribution to derive a mass moment equation set for the cloud microphysical system. In this short study, we go beyond a monodisperse size distribution and explore how the assumption of an exponential particle size distribution affects the condensation/evaporation and collisional growth rates of cloud particles for the mass moment method. In Section 2, we introduce the exponential function and its useful properties when applied to the moment method framework. In Section 3, we derive modifications to the monodisperse size distribution mass condensation/evaporation rates for an exponential distribution. We also propose a tanh function that smoothly interpolates between the continuum/diffusive and free molecular/kinetic regime limits near the critical Knudsen number. In Section 4, we derive expressions for collisional growth for Brownian coagulation and gravitational coalescence. In Section 5, we propose an interpolation function for the settling velocity between the continuum/diffusive and free molecular/kinetic regime limits. In Section 6, we apply our new theory to simple 1D models for a Y-dwarf KCl cloud formation case. Lastly, Sections 7 and 8 respectively contain the discussion and conclusion of our study.

2. Moments with assumed exponential distribution

In this Section, we present a derivation of the mass moments assuming an exponential distribution, as well as derive the source terms required for evolving the cloud formation microphysics ordinary differential equation (ODE) system in time. The exponential distribution, $f(m) [\text{cm}^{-3} \text{ g}^{-1}]$, is a special single parameter form of the gamma distribution given by

$$f(m) = \frac{N_c}{\lambda} e^{-m/\lambda}, \quad (1)$$

where $N_c [\text{cm}^{-3}]$ is the total number density of the distribution, $\lambda [\text{g}]$ is the mean particle mass, which is equal to the expectation

value, $E[m]$, of the distribution, and $m [\text{g}]$, an individual mass in the distribution. The exponential distribution is a favourable distribution when attempting to derive a set of moment equations for a cloud microphysics system due its single parameter and useful analytical properties.

The mass moments of the particle mass distribution, $M^{(k)} [\text{g}^k \text{ cm}^{-3}]$, are given by

$$M^{(k)} = \int_0^\infty m^k f(m) dm, \quad (2)$$

where k is the moment power. Inserting the exponential distribution in the moment equation gives

$$M^{(k)} = \frac{N_c}{\lambda} \int_0^\infty m^k e^{-m/\lambda} dm. \quad (3)$$

After some algebra and applying the definition of the gamma integral¹, the moment generating function for the exponential size distribution is analytically expressed as

$$M^{(k)} = N_c \lambda^k \Gamma(k + 1), \quad (4)$$

where Γ is the gamma function. The moment generating function is useful to close the moment system when required through estimating the higher moment values from lower ones, for example, when calculating the moment dependent settling velocity (e.g. Woitke et al. 2020). Each integer moment represents bulk values of the particle size distribution, such as the total number density, $N_c [\text{cm}^{-3}]$, for $k = 0$

$$M^{(0)} = N_c, \quad (5)$$

and the $k = 1$ moment which represents the total mass density, $\rho_c [\text{g cm}^{-3}]$, of the cloud particles

$$M^{(1)} = \rho_c. \quad (6)$$

The value of λ can be readily estimated from the moment solutions as

$$\lambda = \frac{M^{(1)}}{M^{(0)}} = m_c, \quad (7)$$

which closes the system of equations. Here, following the notation of Lee & Ohno (2025), $m_c [\text{g}]$ is the average mass of the particles. The mean mass weighted average particle size, $r_c [\text{cm}]$, is then

$$r_c = \left(\frac{3m_c}{4\pi\rho_d} \right)^{1/3}, \quad (8)$$

where $\rho_d [\text{g cm}^{-3}]$ is the particle bulk density.

In Figure 1, we show visually the difference between the monodisperse and exponential distributions. From this, it is clear that the monodisperse distribution through its assumption of a single representative grain size places all emphasis on the mean particle size, whereas the exponential distribution is more ‘realistic’ in that there is a variance around the mean particle size. In the exponential distribution, this variance is constant and simply given by the square of the average value

$$\text{Var}[m] = \lambda^2. \quad (9)$$

This single parameter property makes the exponential distribution useful for two moment methods where only the mean particle mass/size can be estimated from the moment solutions. The

¹ $\Gamma(z) = \int_0^\infty t^{z-1} e^{-t} dt$

exponential distribution is characterised by a gradual increase up to the mean particle size, after which the particle number density drops quickly. This places greater emphasis on the small particle population than the monodisperse distribution, a factor that must be considered when modelling physical processes affecting the size distribution. However, this single parameter approach has significant limitations on the flexibility of the size distribution (Section 7).

3. Condensation with exponential distribution

In this Section, we derive the rate of condensation/evaporation of mass from the cloud bulk when assuming an exponential distribution and compare it to the monodisperse derivation. Following the differentiation with time for the method of moments (e.g. Gail & Sedlmayr 2013), the change in time of the moments for the condensation/evaporation process is given by

$$\frac{dM^{(k)}}{dt} = k \int_0^{\infty} m^{k-1} \frac{dm}{dt} f(m) dm, \quad (10)$$

where, dm/dt [g s^{-1}], is the rate of change of the cloud particle mass. In the monodisperse size distribution, the particle size distribution is assumed to be a delta function at the mean particle size expressed formally as

$$f(m) = N_c \delta(m - \lambda). \quad (11)$$

dm/dt is then independent of mass, removing it from the integral in Eq. 10. This leads to the monodisperse moment method typically used in the literature (e.g. Woitke & Helling 2003; Helling et al. 2008; Gail & Sedlmayr 2013; Ohno & Okuzumi 2017; Lee 2023), where the rate of change of a moment k is

$$\frac{dM^{(k)}}{dt} = k \frac{dm}{dt} \int_0^{\infty} m^{k-1} f(m) dm = k \frac{dm}{dt} M^{(k-1)}. \quad (12)$$

For example, the source term for condensational growth/evaporation in the 1st moment ($k = 1$) is

$$\left. \frac{d\rho_c}{dt} \right|_{r_c} = \left. \frac{dm}{dt} \right|_{r_c} N_c, \quad (13)$$

where dm/dt is given by Eq. 16 or 24 dependent on the Knudsen number regime and evaluated at the mean particle size r_c . We define the Knudsen number, Kn, as

$$\text{Kn} = \frac{\lambda_a}{r_c}, \quad (14)$$

where λ_a [cm] is the atmospheric mean path length which can be given by

$$\lambda_a = \frac{2\eta_a}{\rho_a} \sqrt{\frac{\pi\bar{\mu}_a}{8RT}}, \quad (15)$$

with η_a [$\text{g cm}^{-1} \text{s}^{-1}$] the atmospheric dynamical viscosity which be calculated following Lee & Ohno (2025) using the Rosner (2012) fitting function and Davidson (1993) mixing rule, ρ_a [g cm^{-3}] the atmospheric mass density and $\bar{\mu}_a$ [g mol^{-1}] the mean molecular weight of the atmosphere.

For the exponential distribution (and others), unlike for the monodisperse distribution, the mass dependence in the growth rate cannot be ignored in the integral of Eq. 10. The change

in mass for condensation/evaporation in the continuum/diffusive regime ($\text{Kn} \ll 1$) is given by (e.g. Woitke & Helling 2003)

$$\left(\frac{dm}{dt} \right)^{\text{diff}} = 4\pi r D m_0 n_v \left(1 - \frac{1}{S} \right), \quad (16)$$

where r [cm] is the radius of the particle, m_0 [g] the mass of one unit of vapour, n_v [cm^{-3}] the number density of the vapour and S the supersaturation ratio of the vapour. D [$\text{cm}^2 \text{s}^{-1}$] is the diffusive rate of the vapour onto the particle surface and can be given by (e.g. Jacobson 2005)

$$D = \frac{5}{16N_A d_i^2 \rho_a} \sqrt{\frac{RT\bar{\mu}_a}{2\pi} \left(\frac{\mu_v + \bar{\mu}_a}{\mu_v} \right)}, \quad (17)$$

where N_A is Avogadro's number, d_i [cm] the collision diameter, and μ_v [g mol^{-1}] the molecular weight of the condensable vapour.

The particle radius is converted to particle mass through the relation

$$r = \left(\frac{3m}{4\pi\rho_d} \right)^{1/3}, \quad (18)$$

which reveals the mass dependence, $\propto m^{1/3}$, of condensational growth/evaporation in the diffusive/continuum regime. Defining the mass independent kinetic pre-factor as C_0

$$C_0 = 4\pi \left(\frac{3}{4\pi\rho_d} \right)^{1/3} D m_0 n_v \left(1 - \frac{1}{S} \right), \quad (19)$$

equation Eq. 10 becomes

$$\frac{dM^{(k)}}{dt} = k C_0 \int_0^{\infty} m^{1/3} m^{k-1} f(m) dm = k C_0 M^{(k-2/3)}. \quad (20)$$

Using the exponential distribution moment generating function (Eq. 4) this gives

$$\frac{dM^{(k)}}{dt} = k C_0 \lambda^{k-2/3} N_c \Gamma(k + 1/3). \quad (21)$$

We can then use Eq. 4 for the $k - 1$ moment to factor out N_c and get the expression in terms of the previous moment.

$$\frac{dM^{(k)}}{dt} = k C_0 \lambda^{1/3} M^{(k-1)} \frac{\Gamma(k + 1/3)}{\Gamma(k)}. \quad (22)$$

The full expression for the first moment ($k = 1$) is then

$$\left(\frac{d\rho_c}{dt} \right)_{\text{cond}}^{\text{diff}} = 4\pi r_c D m_0 n_v \left(1 - \frac{1}{S} \right) \Gamma(4/3) N_c = \left(\frac{dm}{dt} \right)_{r_c}^{\text{diff}} \Gamma(4/3) N_c, \quad (23)$$

which reveals that the rate of change of the first moment in the $\text{Kn} \ll 1$ regime for the exponential distribution is a factor of $\Gamma(4/3)$ different to the monodisperse rate (Eq. 13).

In the large Knudsen number regime, $\text{Kn} \gg 1$, the free molecular/kinetic regime, the mass dependence is $\propto m^{2/3}$ as the condensation rate expression is given by (e.g. Woitke & Helling 2003)

$$\left(\frac{dm}{dt} \right)^{\text{free}} = 4\pi r^2 v_{\text{th}} m_0 n_v \alpha \left(1 - \frac{1}{S} \right), \quad (24)$$

where $v_{\text{th}} = \sqrt{k_b T / 2\pi m_v}$ [cm s⁻¹] is the thermal velocity of the condensable vapour, with m_v [g] the mass of the condensable vapour. $\alpha = [0,1]$ is the ‘sticking efficiency’ of the vapour to the particle surface. Again, defining the constant kinetic pre-factor C_0 as

$$C_0 = 4\pi \left(\frac{3}{4\pi\rho_d} \right)^{2/3} v_{\text{th}} m_0 n_v \alpha \left(1 - \frac{1}{S} \right), \quad (25)$$

equation Eq. 10 becomes

$$\frac{dM^{(k)}}{dt} = kC_0 \int_0^\infty m^{2/3} m^{k-1} f(m) dm = kC_0 M^{(k-1/3)}. \quad (26)$$

Similar to the $\text{Kn} \ll 1$ regime solution, after using the moment generation function (Eq. 4) the final expression is given as

$$\frac{dM^{(k)}}{dt} = kC_0 \lambda^{k-1/3} N_c \Gamma(k+2/3), \quad (27)$$

and in terms of the $k-1$ moment

$$\frac{dM^{(k)}}{dt} = kC_0 \lambda^{2/3} M^{(k-1)} \frac{\Gamma(k+2/3)}{\Gamma(k)}. \quad (28)$$

This gives for the full first moment ($k=1$) expression

$$\left(\frac{d\rho_c}{dt} \right)_{\text{cond}}^{\text{free}} = 4\pi r_c^2 v_{\text{th}} m_0 n_v \left(1 - \frac{1}{S} \right) \Gamma(5/3) N_c = \left(\frac{dm}{dt} \right)_{r_c}^{\text{free}} \Gamma(5/3) N_c, \quad (29)$$

which reveals that the first moment in the $\text{Kn} \gg 1$ regime is a factor of $\Gamma(5/3)$ different when assuming an exponential size distribution compared to the monodisperse distribution.

Overall, the difference between the monodisperse rate of change and exponential assumed distribution for the first moment is the factors of gamma, $\Gamma(4/3)$ and $\Gamma(5/3)$, which are both < 1 . The rate of condensation in the exponential distribution is therefore a factor ~ 0.9 slower than the monodisperse distribution. This makes intuitive sense, as the monodisperse distribution will weight the number of particles at the mean value compared to the exponential distribution which weights towards more smaller particle representation in its formulation. Combined with the exponential distributions strong drop-off in particle size after the mean value, the condensation rate for the exponential distribution is expected to be lower than the monodisperse distribution.

Our derived analytical solution makes it trivial to include the exponential size particle size dependence in current exoplanet atmosphere cloud condensation codes that use the moment method. Analogous derivations in particle radius or volume space instead of mass are a possibility for theories and models that apply the moments in radius or volume space (e.g. Helling et al. 2008; Gail & Sedlmayr 2013).

3.1. Condensation regime interpolation function

Equations 23 and 29 are valid both in their respective Knudsen number regimes of $\text{Kn} \ll 1$ and $\text{Kn} \gg 1$ respectively. However, in the intermediate regime, $\text{Kn} \sim 1$, a direct expression for the mass condensation/evaporation rate equation is difficult to derive.

To address this, following Woitke & Helling (2003) we apply an interpolation function that transitions smoothly between the

diffusive and free molecular regimes. When the expressions Eq. 23 and Eq. 29 are equal, this results in (Woitke & Helling 2003)

$$\alpha v_{\text{th}} r_c = D, \quad (30)$$

where we have ignored any gamma factors for clarity. Using the Knudsen number definition, the critical Knudsen number, Kn_{cr} , is given by

$$\text{Kn}_{\text{cr}} = \frac{\lambda_a \alpha v_{\text{th}}}{D}. \quad (31)$$

The critical Knudsen number can then be used to interpolate between each regime near the critical value (e.g. Woitke & Helling 2003). We propose a symmetric smooth tanh function of the form

$$f(\text{Kn}') = \frac{1}{2} [1 - \tanh(a \log_{10} \text{Kn}')] \quad (32)$$

where $\text{Kn}' = \text{Kn}/\text{Kn}_{\text{cr}}$ and has a range between 0 and 1. The net change in the first moment is then a linear combination using this interpolation function

$$\left(\frac{d\rho_c}{dt} \right)_{\text{cond}} = f(\text{Kn}') \left. \frac{dm}{dt} \right|_{r_c}^{\text{diff}} N_c + [1 - f(\text{Kn}')] \left. \frac{dm}{dt} \right|_{r_c}^{\text{free}} N_c. \quad (33)$$

We set a scaling value of $a = 2$, which smoothly transitions between the asymptotic expressions at around 2 orders magnitude in Knudsen number away from the critical number. At 1 order of magnitude away from the critical number, the interpolation function gives a value of $f(\text{Kn}') \approx 0.1$ or 0.9 . For consideration of the exponential distribution, the respective gamma factors for each regime can be easily re-included in Eq. 33.

4. Collisional growth with exponential distribution

Another important process in shaping the particle size distribution is the collision and subsequent growth of particles, either through Brownian motion of particles (coagulation) or relative settling velocities of different sized particles (coalescence). In Drake (1972), the mass moment generative function of the Smoluchowski equation for collisional growth is derived as

$$\frac{dM^{(k)}}{dt} = \frac{1}{2} \int_0^\infty \int_0^\infty K(m, m') f(m) f(m') \times [(m+m')^k - m^k - m'^k] dm dm', \quad (34)$$

where m and m' represent different masses in the particle mass distribution and $K(m, m')$ [cm³ s⁻¹] the kernel function. We can immediately find the expression for the zeroth moment as

$$\frac{dM^{(0)}}{dt} = -\frac{1}{2} \int_0^\infty \int_0^\infty K(m, m') f(m) f(m') dm dm', \quad (35)$$

which in general serves as the basis for deriving the collisional growth rate expressions using moment methods.

In Lee & Ohno (2025), following arguments in Rossow (1978), it was assumed that the size distribution is monodisperse, allowing the kernel function to be moved outside the integral. In this study, we apply the method found in Morán & Kholghy (2023, Appendix C) to find size distribution averaged collision kernels, which we repeat below for completeness. Following Eq.

35, in [Morán & Kholghy \(2023\)](#) the number density population averaged collision kernel is given as

$$\begin{aligned} \overline{K(m, m')} &= \frac{\int_0^\infty \int_0^\infty K(m, m') f(m) f(m') dm dm'}{\int_0^\infty \int_0^\infty f(m) f(m') dm dm'} \\ &= \frac{1}{N_c^2} \int_0^\infty \int_0^\infty K(m, m') f(m) f(m') dm dm'. \end{aligned} \quad (36)$$

In the following Sections, we use the [Morán & Kholghy \(2023\)](#) technique to derive population average collision kernels for both the $\text{Kn} \gg 1$ and $\text{Kn} \ll 1$ regimes. We then find collisional growth rate expressions for the monodisperse and exponential distribution cases.

4.1. $\text{Kn} \ll 1$ regime

For collisional growth driven by Brownian motion (coagulation) in the $\text{Kn} \ll 1$ regime, the collisional kernel is given by ([Chandrasekhar 1943](#))

$$K(r, r') = 4\pi [D(r) + D(r')] (r + r'), \quad (37)$$

where r and r' represent different particle radii in the distribution and $D(r)$ is the particle diffusion factor given by ([Chandrasekhar 1943](#))

$$D(r) = \frac{k_b T \beta}{6\pi \eta_a r}, \quad (38)$$

where β , the Cunningham slip factor, generally depends on the radius (and therefore mass) through scaling with Knudsen number in the functional form

$$\beta = 1 + \text{Kn} [A + B e^{-C/\text{Kn}}]. \quad (39)$$

In this study, we use the parameters experimentally measured between $\text{Kn} \approx 0.5$ -83 from [Kim et al. \(2005\)](#)

$$\beta = 1 + \text{Kn} [1.165 + 0.483 e^{-0.997/\text{Kn}}]. \quad (40)$$

Converting Eq. 37 to mass units gives the mass dependence on the kernel

$$K(m, m') = K_0 (m^{-1/3} + m'^{-1/3})(m^{1/3} + m'^{1/3}), \quad (41)$$

where K_0 is the constant kinetic pre-factor given by

$$K_0 = \frac{2k_b T \beta}{3\eta_a}. \quad (42)$$

4.1.1. Monodisperse distribution solution

If we make the monodisperse assumption for the particle mass distribution, where $f(m) \approx N_c \delta(m - \lambda)$ and $f(m') \approx N_c \delta(m' - \lambda)$, the kernel function becomes

$$K(m, m') = 4K_0, \quad (43)$$

leading to a zeroth moment expression given by

$$\frac{dM^{(0)}}{dt} = -2K_0 N_c^2. \quad (44)$$

This results in the same equation from [Lee & Ohno \(2025\)](#) for the number density collisional growth rate

$$\left(\frac{dN_c}{dt} \right)_{\text{coag}} \approx -\frac{4k_b T \beta}{3\eta_a} N_c^2, \quad (45)$$

recovering the monodisperse limit.

4.1.2. Exponential distribution solution

We now attempt a zeroth moment solution assuming an exponential size distribution. Here, we first have to make an assumption about the Cunningham slip factor to make the problem more easily analytically tractable. We therefore assume that β is well expressed at the mean particle mass m_c for both size distributions, and therefore can be taken outside the double integral and subsumed into K_0 . With this assumption, following [Morán & Kholghy \(2023\)](#), the population averaged kernel in this regime is given by

$$\begin{aligned} \overline{K(m, m')} &= \frac{1}{N_c^2} \int_0^\infty \int_0^\infty K(m, m') f(m) f(m') dm dm' \\ &= \frac{K_0}{N_c^2} \int_0^\infty \int_0^\infty (m^{-1/3} + m'^{-1/3})(m^{1/3} + m'^{1/3}) f(m) f(m') dm dm'. \end{aligned} \quad (46)$$

This can be converted into a function of non-integer moment powers as ([Morán & Kholghy 2023](#))

$$\overline{K(m, m')} = \frac{2K_0}{N_c^2} (M^{(0)} M^{(0)} + M^{(1/3)} M^{(-1/3)}), \quad (47)$$

where $M^{(1/3)}$ and $M^{(-1/3)}$ are the $k = 1/3$ and $k = -1/3$ non-integer power moment respectively. Using the moment generating function for the exponential mass distribution (Eq. 4), we can immediately find the population averaged kernel for the exponential distribution in the $\text{Kn} \ll 1$ regime

$$\overline{K(m, m')} = 2K_0 \left[1 + \Gamma\left(\frac{4}{3}\right) \Gamma\left(\frac{2}{3}\right) \right]. \quad (48)$$

Putting this averaged kernel into Eq. 35 gives the change in the number density as

$$\left(\frac{dN_c}{dt} \right)_{\text{coag}} \approx -\frac{2k_b T \beta}{3\eta_a} \left[1 + \Gamma\left(\frac{4}{3}\right) \Gamma\left(\frac{2}{3}\right) \right] N_c^2. \quad (49)$$

Evaluating the bracket containing the gamma functions gives ≈ 2.21 , meaning the rate of change of number density from collisional growth assuming an exponential distribution is therefore around ≈ 1.1 times larger than the monodisperse assumption in the $\text{Kn} \ll 1$ regime.

4.2. $\text{Kn} \gg 1$ regime

For Brownian coagulation in the $\text{Kn} \gg 1$ regime, the collisional kernel is given by ([Jacobson 2005](#))

$$K(r, r') = \pi (r + r')^2 \sqrt{(v(m)^2 + v(m')^2)}, \quad (50)$$

where v is the thermal velocity of the particle given by

$$v = \sqrt{\frac{8k_b T}{\pi m}}. \quad (51)$$

Converting the kernel to mass units gives

$$K(m, m') = K_0 (m^{1/3} + m'^{1/3})^2 \sqrt{\left(\frac{1}{m} + \frac{1}{m'} \right)}, \quad (52)$$

where K_0 is the kinetic pre-factor

$$K_0 = \left(\frac{3}{4\pi\rho} \right)^{2/3} \sqrt{8\pi k_b T}. \quad (53)$$

4.2.1. Monodisperse solution

For the monodisperse solution, the mass distribution takes the form $f(m) \approx N_c \delta(m - \lambda)$ and $f(m') \approx N_c \delta(m' - \lambda)$. The kernel now becomes

$$K(m, m') = 4 \sqrt{\frac{2}{\lambda}} K_0 \lambda^{2/3}. \quad (54)$$

Leading to a zeroth moment expression as

$$\frac{dM^{(0)}}{dt} = -2 \sqrt{\frac{2}{\lambda}} K_0 \lambda^{2/3}. \quad (55)$$

The full equation for the coagulation rate is then

$$\left(\frac{dN_c}{dt}\right)_{\text{coag}} \approx -2 \sqrt{\frac{2}{\lambda}} \left(\frac{3}{4\pi\rho}\right)^{2/3} \sqrt{8\pi k_b T} m_c^{2/3} N_c^2, \quad (56)$$

and simplifies to

$$\left(\frac{dN_c}{dt}\right)_{\text{coag}} \approx -8 \sqrt{\frac{\pi k_b T}{m_c}} r_c^2 N_c^2, \quad (57)$$

which is the same expression found in previous monodisperse studies (e.g. Lee & Ohno 2025).

4.2.2. Exponential distribution solution

Finding a fully consistent analytical solution assuming an exponential distribution is difficult in this regime, but we can follow the same method in Morán & Kholghy (2023) to derive a population averaged kernel function. Placing Eq. 52 into Eq. 36 gives

$$\begin{aligned} \overline{K(m, m')} &= \frac{1}{N_c^2} \int_0^\infty \int_0^\infty K(m, m') f(m) f(m') dm dm' \\ &= \frac{K_0}{N_c^2} \\ &\int_0^\infty \int_0^\infty (m^{1/3} + m'^{1/3})^2 (m^{-1/2} + m'^{-1/2}) f(m) f(m') dm dm'. \end{aligned} \quad (58)$$

This results in a set of six integrals, the solutions of which are non-integer powers of the moments. After integrating and some algebra, the end result is

$$\overline{K(m, m')} = \frac{2K_0}{N_c^2} \left(M^{(2/3)} M^{(-1/2)} + 2M^{(1/3)} M^{(-1/6)} + M^{(1/6)} M^{(0)} \right), \quad (59)$$

where $M^{(2/3)}$, $M^{(-1/2)}$, $M^{(1/3)}$, $M^{(-1/6)}$ and $M^{(1/6)}$ are the $k = 2/3$, $k = -1/2$, $k = 1/3$, $k = -1/6$ and $k = 1/6$ non-integer powers of the moments respectively. Using the moment generating function for the exponential mass distribution (Eq. 4), results in

$$\overline{K(m, m')} = 2K_0 \lambda^{1/6} \left[\Gamma\left(\frac{5}{3}\right) \Gamma\left(\frac{1}{2}\right) + 2\Gamma\left(\frac{4}{3}\right) \Gamma\left(\frac{5}{6}\right) + \Gamma\left(\frac{7}{6}\right) \right]. \quad (60)$$

Using the relation $\lambda^{1/6} = \lambda^{2/3} \lambda^{-1/2}$, the final expression for the change in number density can be given in a similar form to the monodisperse relation

$$\left(\frac{dN_c}{dt}\right)_{\text{coag}} \approx -\sqrt{\frac{8\pi k_b T}{m_c}} r_c^2 N_c^2 \left[\Gamma\left(\frac{5}{3}\right) \Gamma\left(\frac{1}{2}\right) + 2\Gamma\left(\frac{4}{3}\right) \Gamma\left(\frac{5}{6}\right) + \Gamma\left(\frac{7}{6}\right) \right] \quad (61)$$

Overall, the exponential distribution collision rate is a factor of ≈ 1.6 faster than the monodisperse formulation in the $\text{Kn} \gg 1$ regime.

4.3. Collisional regime interpolation function

Equations 49 and 61 are valid in the $\text{Kn} \ll 1$ and $\text{Kn} \gg 1$ limits respectively, however, in many cases particles occupy an intermediate regime $\text{Kn} \sim 1$ where it is difficult to derive an analytical Brownian coagulation kernel. To solve this problem, many studies apply an interpolation function between the limiting regimes, with the most common following the Fuchs (1964) prescription (e.g. Lavvas et al. 2011; Gao et al. 2018).

In this study, we follow Morán (2022) who propose a simple and accurate interpolation function between the continuum/diffusive ($\text{Kn} \ll 1$) and free molecular/kinetic ($\text{Kn} \gg 1$). This is designed as a modification to the diffusive regime kernel as

$$K(r, r') = 4\pi [D(r) + D(r')] (r + r') g(\text{Kn}_D), \quad (62)$$

where Kn_D is the diffusive particle Knudsen number given by

$$\text{Kn}_D = \frac{8\sqrt{2} [D(r) + D(r')]}{\pi \sqrt{v(r)^2 + v(r')^2} (r + r')}, \quad (63)$$

for a particle size pair. The interpolation function, $g(\text{Kn}_D)$, derived in Morán (2022) is stated as

$$g(\text{Kn}_D) = \left(1 + \frac{\pi^2}{8} \text{Kn}_D^2 \right)^{-1/2}, \quad (64)$$

which varies between a value of 1 for the diffusive/continuum regime as $\text{Kn}_D \rightarrow 0$ and recovers the kinetic/free molecular kernel as $\text{Kn}_D \rightarrow \infty$. We can calculate a population averaged diffusive particle Knudsen number $\overline{\text{Kn}_D}$ using the population averaged kernels

$$\overline{\text{Kn}_D} = \frac{2\sqrt{2} \overline{K_1(m, m')}}{\pi \overline{K_h(m, m')}}, \quad (65)$$

where $\overline{K_1(m, m')}$ is the population averaged kernel for the $\text{Kn} \ll 1$ regime from Eq. 48 and $\overline{K_h(m, m')}$ is the population averaged kernel for the $\text{Kn} \gg 1$ regime from Eq. 60.

For a monodisperse size distribution, this interpolation function can be readily used to modify Eq. 45

$$\left(\frac{dN_c}{dt}\right)_{\text{coag}} \approx -\frac{4k_b T \beta}{3\eta_a} N_c^2 g(\text{Kn}_D), \quad (66)$$

where Kn_D is evaluated at the mean grain size. For the exponential distribution, this results in the coagulation rate given as

$$\left(\frac{dN_c}{dt}\right)_{\text{coag}} \approx -\frac{2k_b T \beta}{3\eta_a} \left[1 + \Gamma\left(\frac{2}{3}\right) \Gamma\left(\frac{4}{3}\right) \right] N_c^2 g(\overline{\text{Kn}_D}), \quad (67)$$

which recovers the $\text{Kn} \gg 1$ and $\text{Kn} \ll 1$ collisional rate limits for the exponential distribution.

4.4. Gravitational coalescence

For gravitational coalescence, the collisional growth kernel is given by (e.g. Jacobson 2005)

$$K(r, r') = \pi (r + r')^2 |v_f(r) - v_f(r')| E, \quad (68)$$

where v_f [cm s⁻¹] is the settling velocity of the particle. Defining $\Delta v_f = |v_f(r) - v_f(r')|$ we follow Ohno & Okuzumi (2017) and

evaluate Δv_f with a parameter, ϵ , that estimates the relative velocity of the particles from the mean particle size settling velocity, $v_f(r_c)$, giving $\Delta v_f \approx \epsilon v_f(r_c)$. This is taken as $\epsilon \approx 0.5$ following the results of [Sato et al. \(2016\)](#), who found this value to best reproduce the results of a collisional bin resolving model for grain growth in protoplanetary disks.

E is a collisional efficiency factor, dependent on the Stokes number, Stk ,

$$\text{Stk} = \frac{\Delta v_f v_f(r_c)}{gr_c} = \frac{\epsilon v_f^2(r_c)}{gr_c}. \quad (69)$$

E is then given by ([Guillot et al. 2014](#))

$$E = \begin{cases} \max[0, 1 - 0.42\text{Stk}^{-0.75}] & \text{Kn} < 1 \\ 1 & \text{Kn} \geq 1 \end{cases} \quad (70)$$

4.4.1. Monodisperse solution

For the monodisperse distribution, putting the kernel from Eq. 68 into Eq. 35 and evaluating at the mean particle size, leads to the expression found in previous studies (e.g. [Lee & Ohno 2025](#))

$$\left(\frac{dN_c}{dt}\right)_{\text{coal}} \approx -2\pi r_c^2 \Delta v_f E N_c^2. \quad (71)$$

4.4.2. Exponential distribution

For an exponential distribution, we make the assumption that Δv_f and E are well defined at the mean particle size value, allowing them to be taken outside the integral, making the integral analytically more tractable. Defining the kinetic pre-factor as

$$K_0 = \left(\frac{3}{4\pi\rho}\right)^{2/3} \pi \Delta v_f E, \quad (72)$$

the population averaged kernel is expressed as

$$\begin{aligned} \overline{K(m, m')} &= \frac{1}{N_c^2} \int_0^\infty \int_0^\infty K(m, m') f(m) f(m') dm dm' \\ &= \frac{K_0}{N_c^2} \int_0^\infty \int_0^\infty (m^{1/3} + m'^{1/3})^2 f(m) f(m') dm dm'. \end{aligned} \quad (73)$$

Solving the integral results in

$$\overline{K(m, m')} = \frac{2K_0}{N_c^2} \left(M^{(2/3)} M^{(0)} + M^{(1/3)} M^{(1/3)} \right). \quad (74)$$

In the same procedure as the coagulation kernels, assuming an exponential distribution results in the final expression being

$$\left(\frac{dN_c}{dt}\right)_{\text{coal}} \approx -\pi r_c^2 \Delta v_f E N_c^2 \left[\Gamma\left(\frac{5}{3}\right) + \Gamma\left(\frac{4}{3}\right)^2 \right]. \quad (75)$$

Overall, the collisional growth rate from gravitational coalescence assuming an exponential distribution is ≈ 0.85 times slower than the monodisperse approximation.

4.5. Summary of collisional growth results

Similar to the condensation factor of 0.9, the 1.1 enhancement factor for Brownian motion in the $\text{Kn} \ll 1$ regime makes intuitive sense for the exponential distribution as the distribution is more skewed towards smaller particles with an exponential drop-off for particle larger than the mean particle size. The collision rate is therefore enhanced due to the consideration of the smaller particle population in the exponential distribution. For the $\text{Kn} \gg 1$ regime, the increase by ~ 1.6 also makes intuitive sense, as in this regime collisions are guided by the relative cross-section of the particles which is reduced for smaller particles but more strongly counteracted by the increased thermal velocity of small particles. Similarly, for gravitational coalescence, the collisional rate is dependent on the relative cross-section of the particles, resulting in an overall reduction in collisional growth rate of around ≈ 0.85 for the exponential distribution compared to the monodisperse distribution.

5. Settling velocity interpolation function

In the $\text{Kn} \ll 1$ regime, the Stokes law with included Reynolds number dependent fitting factor can be used from [Ohno & Okuzumi \(2018\)](#)

$$v_f(r) = \frac{2\beta gr^2(\rho_d - \rho_a)}{9\eta_a} \left[1 + \left(\frac{0.45gr^3\rho_a\rho_d}{54\eta_a^2} \right)^{2/5} \right]^{-5/4}, \quad (76)$$

where here we have re-included the additional buoyancy term from the original Stokes law derivation. However, in the $\text{Kn} \gg 1$ regime, which is commonly a regime where small particles in exoplanet atmospheres are found, the Epstein regime drag law should be used. Here, we can follow [Woitke & Helling \(2003\)](#) who used the [Schaaf \(1963\)](#) drag coefficients in the limiting case for settling velocities well below the atmospheric thermal velocity, $v_f \ll c_T$, to derive

$$v_f(r) = \frac{\sqrt{\pi} g \rho_d r}{2\rho c_T}, \quad (77)$$

where $c_T = \sqrt{2k_b T/m_a}$ [cm s⁻¹] is the thermal velocity of the atmosphere.

We can again use the same tanh function from Eq. 32 to smoothly interpolate between the two expressions

$$v_f = f(\text{Kn}') v_{f,\text{Stokes}} + [1 - f(\text{Kn}')] v_{f,\text{Epstein}}, \quad (78)$$

where $\text{Kn}' = \text{Kn}/\text{Kn}_{\text{cr}}$. Choosing a suitable critical value for the settling velocity transition region is a tricky endeavor, for example, [Woitke & Helling \(2003\)](#) find a critical value of $\text{Kn}_{\text{cr}} = 1/3$ equating limits of their drag force derivations. Through trial and error and visual inspection, we find that $\text{Kn}_{\text{cr}} = 1$ with a scaling factor of $a = 2$ gives a good balance and smooth transition for the Knudsen number regime limit velocities.

6. Y-dwarf KCl cloud simple 1D example

In this Section, we apply our new equation set to a simple 1D KCl Y-dwarf example. We follow the same setup from [Gao et al. \(2018\)](#), taking their Y-dwarf temperature-pressure (T-p) profiles, $\log g$ and constant K_{zz} parameters used in their study. We use a simple, second order explicit 1D vertical diffusion and advection time stepping scheme, similar to that used in recent ExoFMS GCM simulations of brown dwarfs ([Lee et al. 2024; Lee](#)

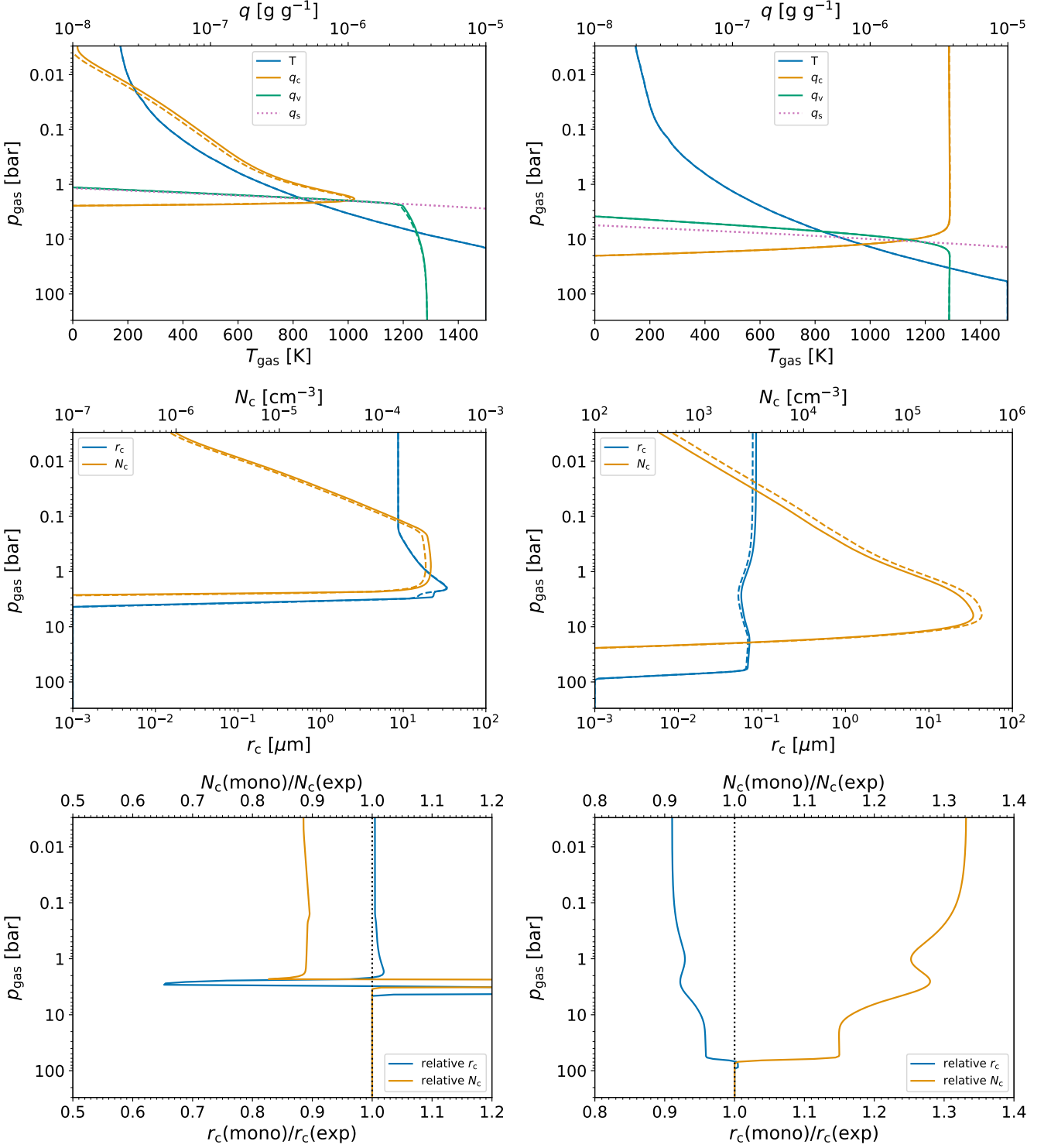


Fig. 2. KCl cloud structures using the $\log g = 3.25$ (left) and $\log g = 4.25$ (right) Y-dwarf temperature-pressure profiles from [Gao et al. \(2018\)](#) and assuming a constant $K_{zz} = 10^8 \text{ cm}^2 \text{ s}^{-1}$. The dashed lines show the monodisperse size distribution and the solid lines the exponential size distribution results. The top panel shows the temperature-pressure profiles with the mass mixing ratio of the condensate, q_c , vapour, q_v and saturation point, q_s . The middle panel shows the mean particle size, r_c , and total number density, N_c . The bottom panel shows the relative difference in r_c and N_c between the monodisperse and exponential cloud structure.

& Ohno 2025). For the cloud microphysics, we use the ODE system presented in [Lee & Ohno \(2025\)](#) which includes condensation/evaporation, collisional growth and homogeneous nucleation, but with the modifications for the exponential distribution rates from this study when appropriate. We assume that the settling velocity for each moment is well defined at the mass

weighted radius (Eq. 8) as derived from the moment solutions at each timestep. We also assume that the particles are well coupled to the turbulent flow, and so are also vertically diffused in the atmosphere at the given K_{zz} eddy diffusion coefficient (e.g [Woitke et al. 2020](#)). We integrate the 1D column in time for 10^9

seconds, after which all variables show relative differences less than 10^{-6} between timesteps.

Figure 2 shows our results for the 1D column model. In the $\log g = 3.25$ case, we find a near constant $\sim 12\%$ increase in total number density in the exponential distribution compared to the monodisperse distribution, however, the mean particle sizes only differ by 1-2%. We suggest that, due to the mean particle size being quite large in this case, $\sim 10 \mu\text{m}$, this difference in number density arises from the change in the gravitational coalescence rate between the monodisperse and exponential distributions, with the slower rate in the exponential case overall leading to a larger number density inside the cloud layer. Since the difference is not precisely 0.85, as suggested by our gravitational coalescence results, we suggest that, in this case, the enhancement factor of ~ 1.1 in the $\text{Kn} \ll 1$ regime for coagulation somewhat offsets the lower collision rate from gravitational coalescence.

In the $\log g = 4.25$ case, larger differences are seen between the size distribution assumptions, with around a 20-40% reduction in cloud particle number density in the exponential case compared to the monodisperse case. Due to the small mean particle size of $\sim 0.1 \mu\text{m}$, this suggests that the 1.6 factor in the $\text{Kn} \gg 1$ regime for coagulation is responsible for this difference. A $\sim 10\%$ relative difference is seen in mean particle radius.

In both size distribution cases, the mass mixing ratio and vapour mixing ratio profile remain highly similar. This suggests that the total mass that is condensed is not markedly altered between each assumption, but the balance in mass distributed between number density and particle size is changed.

7. Discussion

Several assumptions were made to simplify the coagulation collisional growth integrals analytically. Specifically, in the $\text{Kn} \ll 1$ regime we assumed the Cunningham slip factor was well defined at the mean particle size which is generally not the case, especially for a broad distribution where the slip factor can be significant for the larger particle population. In the $\text{Kn} \gg 1$ regime, no further assumptions were required to produce a solution. For gravitational coalescence, we assumed the collisional efficiency factor was well defined at the mean particle size. However, this assumption may not be entirely accurate, particularly in the $\text{Kn} < 1$ regime, where efficiency factors can vary widely, including reaching zero. Should the efficiency factor vary significantly from the average value across the size distribution, we can expect a significantly altered overall coalescence rate to those presented here. Accounting for these additional effects analytically or through a numerical or interpolation approach and relaxing the assumptions may be possible in the future, but is beyond the scope of the current study.

Our assumption of an exponential size distribution has many limitations, especially when compared to more flexible size distributions such as the gamma or log-normal distribution. The single parameter limitation of the exponential distribution inherits the assumption that the overall particle size distribution shape does not change in time, with the variance remaining constant at the square of the average particle mass at across the time evolution of the cloud structure. The gamma and log-normal distribution contain an additional parameter compared to the one-parameter exponential distribution, allowing them to capture a much less strict and flexible size distribution shape. A major advantage of the more complex distributions would be the allowance of the representation of both narrow and broad size distributions through directly calculating the variance using the mo-

ment results, rather than the assumed variance of the exponential distribution. To visualise the exponential distribution limitations, in Figure 3 we show the reconstructed exponential distributions for the results in Section 6 that used the exponential equation set from this study. From this, it is clear that the overall shape of the distribution does not change much across the cloud structure, a direct result of the assumed variance in the exponential distribution, meaning representation of a narrower or broader size distribution is limited in the exponential distribution. This can be compared to when the variance can be flexible, for example, Helling et al. (2008) reconstruct a potential exponential distribution with narrow and broad distributions with height. However, it should be noted that Helling et al. (2008) reconstructed the size-distribution from a monodisperse microphysics method.

However, with its useful analytical properties and single parameter enabling a two-moment representation, rather than three or more moments for the more complex distributions, the exponential distribution offers a simple way to attempt to take into account polydispersity in the size distribution. With the equations presented here, modellers can be more self-consistent in exploring the effects of polydispersity, rather than reconstructing distributions from moment solutions obtained from the monodisperse equation set (e.g. Helling et al. 2008; Stark et al. 2015; Lee 2023). Since the exponential distribution is a special parameterised form of the gamma distribution, we suspect that designing a three-moment framework with the gamma distribution will take a similar form to that derived here but with additional correction terms to the monodisperse equation set.

Our results in Section 6 used the same Y-dwarf T-p profiles as Gao et al. (2018), which also allows us to compare the moment method results to the 1D CARMA bin-resolving model used in Gao et al. (2018) who also modelled pure KCl cloud particle formation. Despite the exact detailed condensation, nucleation and collisional growth equations being different between this study and those in Gao et al. (2018), this serves as a useful comparison between both methodologies. From the results in Gao et al. (2018) in the $\log g = 3.25$ case the results between the presented moment method and CARMA are remarkably similar. Both models show a very similar condensed mass fraction structure. The mean particle size also shows good agreement in this case, hovering around the $10 \mu\text{m}$ range, but the CARMA results tend to produce slightly smaller particles in the upper atmosphere by a few factors in this case. However, it is difficult to one-to-one compare, since Gao et al. (2018) present the effective particle radius (weighted by area) whereas our results show the mass weighted radius (weighted by mass/volume). Despite this, our results are quite consistent as the effective particle radius is always smaller than the mass weighted radius by some factor in a particle size distribution. In the $\log g = 4.25$ case, our results are much more different to Gao et al. (2018), in particular Gao et al. (2018) shows a near constant effective particle radius of around $3 \mu\text{m}$ whereas we produce particles at around $\sim 0.08 \mu\text{m}$. We suggest that this may be a case where the bin model produces a bimodal distribution, where the particle size distribution is split between a small particle regime and large particle regime, not able to be captured by the current moment methodology. This skews the effective particle radius to the large particle population in the bin model, even if they are significantly less in number density. We suspect that the moment method is capturing the small particle regime in this case but is unable to model the large particle population due to the assumption of a continuous distribution inherent in the method.

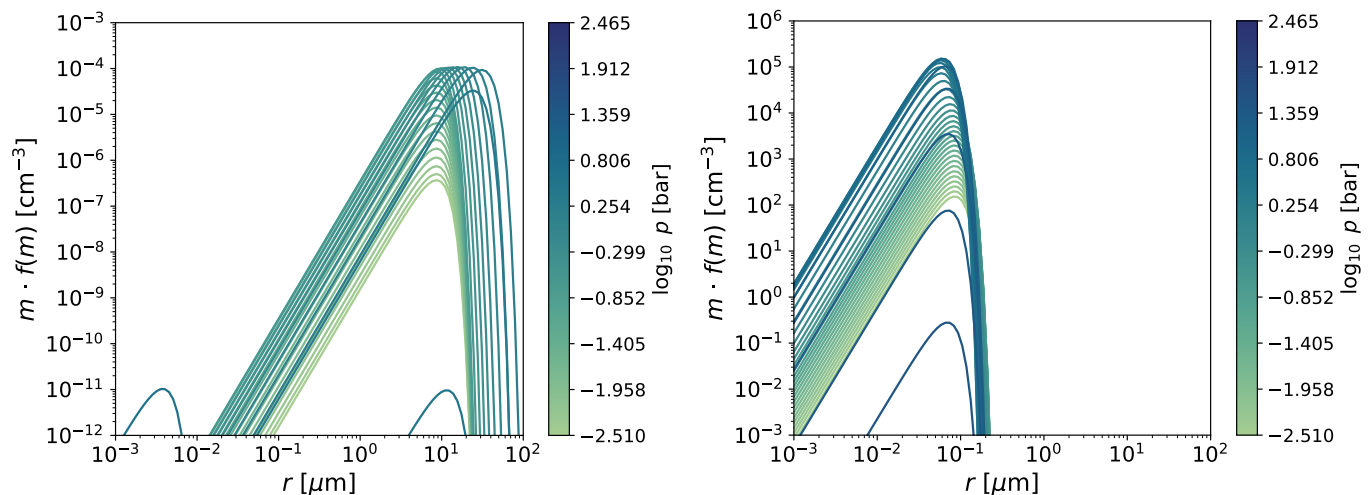


Fig. 3. Reconstructed exponential particle size distributions (Eq. 1) from the Y-dwarf KCl case moment results (Left: $\log g = 3.25$, Right: $\log g = 4.25$) in Section 6 when the exponential distribution is assumed. The colour bar shows the atmospheric pressure of the distribution. This shows the limitations of the exponential distribution as limited flexibility is present due to the assumed variance, resulting in a highly similar distribution shape across the cloud layer.

8. Conclusions

In this short paper, we derived condensation/evaporation and collisional growth expressions for a two moment cloud microphysical scheme applicable to sub-stellar atmospheric clouds. We went beyond the non-disperse assumptions commonly used in previous studies and found simple analytical and tractable solutions when assuming an exponential particle size distribution.

Our analysis found that assuming an exponential distribution for particles leads to simple analytical formulae, which, in effect, modify the monodisperse formulations with constant factors for the time dependent moment equations. These are ≈ 0.9 for the condensation/evaporation rate (first moment) and ≈ 1.1 for Brownian collisional growth (zeroth moment) in the $\text{Kn} \ll 1$ regime and ≈ 1.6 for Brownian collisional growth in the $\text{Kn} \gg 1$ regime and ≈ 0.85 for the gravitational coalescence collisional rate. However, we note that several simplifying assumptions were made regarding integrating the collision growth equations in order to make the problem more analytically tractable. In addition, we proposed simple interpolation functions for evaluating the condensation, settling velocity and collisional growth rates in the $\text{Kn} \sim 1$ transition regime.

In a simple 1D column model example, we found maximum differences of a factor of $\sim 40\%$ in number density and $\sim 10\%$ in particle size between the monodisperse and exponential size distribution assumptions. We suggest that, in our particular cases, the total condensed mass in the cloud structure is similar between each assumption, but the balance between number density and mean particle sizes are affected by the choice of size distribution assumption.

In future papers, we will extend our two moment framework to three moments to enable self-consistent evolution of more complex, three parameter, size distributions, but are still somewhat analytically tractable, such as the log-normal and gamma distributions. Due to the exponential distribution case being a special case of the gamma distribution, we find it likely that derivations using the gamma distribution will follow similar structure to the equations presented in this study.

Acknowledgements. E.K.H. Lee is supported by the CSH through the Bernoulli Fellowship. We thank K. Ohno for initial discussions on the topic.

References

- Chandrasekhar, S. 1943, *Reviews of Modern Physics*, 15, 1
- Davidson, T. 1993, *A Simple and Accurate Method for Calculating Viscosity of Gaseous Mixtures*, Report of investigations (U.S. Department of the Interior, Bureau of Mines)
- Drake, R. L. 1972, *Journal of the Atmospheric Sciences*, 29, 537
- Fuchs, N. 1964, *The Mechanics of Aerosols*, Dover books on engineering (Dover Publications)
- Gail, H.-P. & Sedlmayr, E. 2013, *Physics and Chemistry of Circumstellar Dust Shells*, Cambridge Astrophysics (Cambridge University Press)
- Gao, P., Marley, M. S., & Ackerman, A. S. 2018, *ApJ*, 855, 86
- Guillot, T., Ida, S., & Ormel, C. W. 2014, *A&A*, 572, A72
- Helling, C., Woitke, P., & Thi, W. F. 2008, *A&A*, 485, 547
- Hong, S.-Y. & Lim, J.-O. J. 2006, *Asia-Pacific Journal of Atmospheric Sciences*, 42, 129
- Jacobson, M. Z. 2005, *Fundamentals of Atmospheric Modeling*, 2nd edn. (Cambridge University Press)
- Kim, J., Mulholland, G., Kukuck, S., & Pui, D. 2005
- Lavvas, P., Griffith, C. A., & Yelle, R. V. 2011, *Icarus*, 215, 732
- Lee, E., Dobbs-Dixon, I., Helling, C., Bognar, K., & Woitke, P. 2016, *A&A*, 594, A48
- Lee, E. K. H. 2023, *MNRAS*, 524, 2918
- Lee, E. K. H. & Ohno, K. 2025, *A&A*, 695, A111
- Lee, E. K. H., Tan, X., & Tsai, S.-M. 2024, *MNRAS*, 529, 2686
- Lin, Y.-L., Farley, R. D., & Orville, H. D. 1983, *Journal of Applied Meteorology*, 22, 1065
- Lines, S., Mayne, N. J., Boutle, I. A., et al. 2018, *A&A*, 615, A97
- Marshall, J. S. & Palmer, W. M. K. 1948, *Journal of Atmospheric Sciences*, 5, 165
- Morán, J. & Kholghy, M. R. 2023, *Aerosol Science Technology*, 57, 782
- Morrison, H., van Lier-Walqui, M., Fridlind, A. M., et al. 2020, *Journal of Advances in Modeling Earth Systems*, 12, e2019MS001689, e2019MS001689
- Morán, J. 2022, *Fractal and Fractional*, 6
- Ohno, K. & Okuzumi, S. 2017, *ApJ*, 835, 261
- Ohno, K. & Okuzumi, S. 2018, *ApJ*, 859, 34
- Powell, D., Loudon, T., Kreidberg, L., et al. 2019, *ApJ*, 887, 170
- Pruppacher, H. R. & Klett, J. D. 1978, *Microphysics of Clouds and Precipitation* (Springer Dordrecht)
- Rosner, D. E. 2012, *Transport processes in chemically reacting flow systems* (Courier Corporation)
- Rosow, W. B. 1978, *Icarus*, 36, 1
- Sato, T., Okuzumi, S., & Ida, S. 2016, *A&A*, 589, A15
- Schaaf, S. A. 1963, *Handbuch der Physik*, 3, 591
- Seifert, A. 2008, *COSMO Newsletter*, 7, 25
- Stark, C. R., Helling, C., & Diver, D. A. 2015, *A&A*, 579, A41
- Tan, X. & Showman, A. P. 2019, *ApJ*, 874, 111
- Woitke, P. & Helling, C. 2003, *A&A*, 399, 297
- Woitke, P. & Helling, C. 2004, *A&A*, 414, 335
- Woitke, P., Helling, C., & Gunn, O. 2020, *A&A*, 634, A23